Cell Stem Cell, Volume *28*

Supplemental Information

Principles of signaling pathway modulation for enhancing human naive pluripotency induction

Jonathan Bayerl, Muneef Ayyash, Tom Shani, Yair Shlomo Manor, Ohad Gafni, Rada Massarwa, Yael Kalma, Alejandro Aguilera-Castrejon, Mirie Zerbib, Hadar Amir, Daoud Sheban, Shay Geula, Nofar Mor, Leehee Weinberger, Segev Naveh Tassa, Vladislav Krupalnik, Bernardo Oldak, Nir Livnat, Shadi Tarazi, Shadi Tawil, Emilie Wildschutz, Shahd Ashouokhi, Lior Lasman, Varda Rotter, Suhair Hanna, Dalit Ben-Yosef, Noa Novershtern, Sergey Viukov, and Jacob H. Hanna

Cell Stem Cell, Volume *28*

Supplemental Information

Principles of signaling pathway modulation for enhancing human naive pluripotency induction

Jonathan Bayerl, Muneef Ayyash, Tom Shani, Yair Manor, Ohad Gafni, Rada Massarwa, Yael Kalma, Alejandro Aguilera-Castrejon, Mirie Zerbib, Hadar Amir, Daoud Sheban, Shay Geula, Nofar Mor, Leehee Weinberger, Segev Naveh-Tassa, Vladislav Krupalnik, Bernardo Oldak, Nir Livnat, Shadi Tarazi, Shadi Tawil, Emilie Wildschutz, Shahd Ashouokhi, Lior Lasman, Varda Rotter, Suhair Hanna, Dalit Ben-Yosef, Noa Novershtern, Sergey Viukov, and Jacob H. Hanna

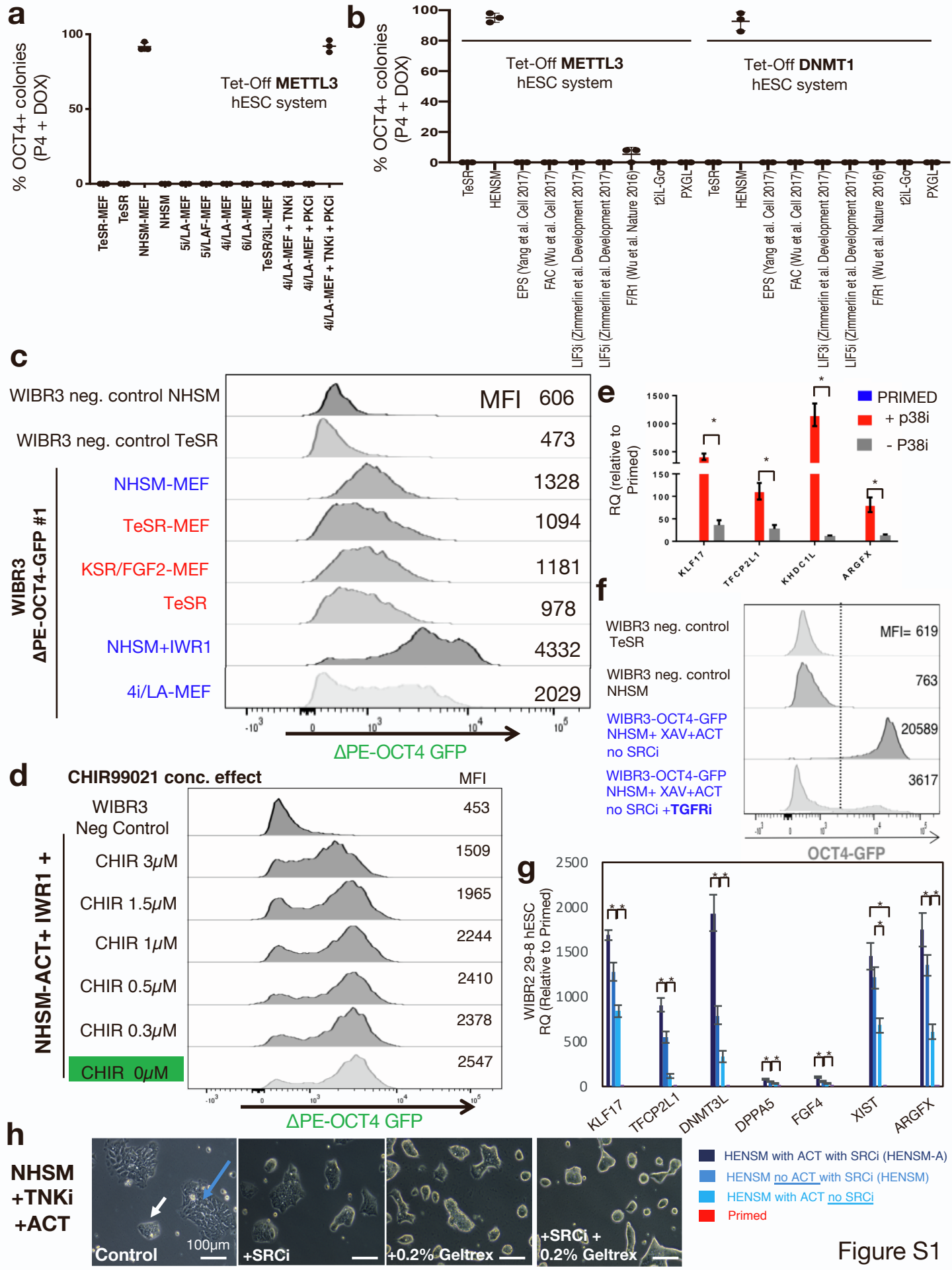
a
% OCT4+ colonies (P4 + DOX)
Tet-Off METTL3 hESC system
TeSR-MEF
TeSR
NHSM-MEF
NHSM
5i/LA-MEF
5i/LAF-MEF
4i/LA-MEF
6i/LA-MEF
TeSR/3iL-MEF
4i/LA-MEF + TNKi
4i/LA-MEF + PKCi
4i/LA-MEF + TNKi + PKCi
b
% OCT4+ colonies (P4 + DOX)
Tet-Off METTL3 hESC system
Tet-Off DNMT1 hESC system
TeSR
HENSM
EPS (Yang et al. Cell 2017)
FAC (Wu et al. Cell 2017)
LIF3i (Zimmerlin et al. Development 2017)
LIF5i (Zimmerlin et al. Development 2017)
F/R1 (Wu et al. Nature 2016)
t2iL-Go
PXGL
c
WIBR3 ΔPE-OCT4-GFP #1
WIBR3 neg. control NHSM
WIBR3 neg. control TeSR
NHSM-MEF
TeSR-MEF
KSR/FGF2-MEF
TeSR
NHSM+IWR1
4i/LA-MEF
MFI
606
473
1328
1094
1181
978
4332
2029
ΔPE-OCT4 GFP
d
NHSM-ACT+ IWR1 +
CHIR99021 conc. effect
MFI
WIBR3 Neg Control
CHIR 3μM
CHIR 1.5μM
CHIR 1μM
CHIR 0.5μM
CHIR 0.3μM
CHIR 0μM
453
1509
1965
2244
2410
2378
2547
ΔPE-OCT4 GFP
e
RQ (relative to Primed)
PRIMED
+ p38i
- P38i
KLF17
TFCP2L1
KHDC1L
ARGFX
f
WIBR3 neg. control TeSR
WIBR3 neg. control NHSM
WIBR3-OCT4-GFP NHSM+ XAV+ACT no SRCi
WIBR3-OCT4-GFP NHSM+ XAV+ACT no SRCi +TGFRi
MFI= 619
763
20589
3617
OCT4-GFP
g
WIBR2 29-8 hESC RQ (Relative to Primed)
KLF17
TFCP2L1
DNMT3L
DPPA5
FGF4
XIST
ARGFX
h
NHSM +TNKi +ACT
Control
100μm
+SRCi
+0.2% Geltrex
+SRCi + 0.2% Geltrex
HENSM with ACT with SRCi (HENSM-A)
HENSM no ACT with SRCi (HENSM)
HENSM with ACT no SRCi
Primed

Figure S1

Figure S1. Reporter systems for screening for enhanced human naive pluripotency conditions. Related to Figure 1.

a. W3G4 METTL3 TET-OFF cells were transitioned in the presence of DOX in the indicated growth conditions for up to 4 passages and stained for OCT4 to quantify percentage of cells that retained their pluripotency. Graph shows that NHSM conditions without feeder cells and other previously described naïve and primed conditions for human ESCs/iPSCs failed to maintain pluripotency in majority of cells expanded in the presence of Dox. **b.** METTL3 TET-OFF and DNMT1 TET-OFF primed cells were transitioned in the presence of DOX for up to 4 passages in different previously published naïve and primed conditions and stained for OCT4 to quantify percentage of cells that retained their pluripotency. **c**. FACS quantification of ΔPE-OCT4-GFP knock in naïve pluripotency reporter, in variety of primed (red) and naïve conditions (blue). Mean fluorescence intensity values (MFI) are indicated. Figure shows that supplementing NHSM conditions with TNKi like IWR1 small molecules boosts expression of GFP suggesting enhancement of naivety characteristics. **d**. Quantification of ΔPE-OCT4-GFP knock in naïve pluripotency reporter, in optimized naïve conditions and various concentrations of GSK3 inhibitor that leads to WNT activation (CHIR99021 is used as GSK3 inhibitor and is abbreviated as CHIR). Figure indicates that CHIR addition negatively influences human naive pluripotency as determined by ΔPE-OCT4-GFP intensity. **e.** RT-PCR analysis for naïve pluripotency markers in HENSM conditions with and without P38i/JNKi (BIRB0796). Values were normalized to ACTIN and values in primed conditions were set as 1. *t-test *p* Value < 0.01. **f.** FACS analysis for OCT4-GFP pluripotency reporter expression following addition of TGFRi. In optimized NHSM conditions that still lack SRCi, pluripotency is rapidly lost upon inhibition of TGFRi. **g**. RT-PCR analysis for naïve pluripotency markers in the indicated HENSM conditions with and without ACTIVIN or SRCi. Values were normalized to ACTIN and values in primed conditions were set as 1. *t-test *p* Value < 0.01. **h.** Phase-contrast images showing how supplementation of 0.2% Geltrex (Life Technologies) in the growth media and SRCi additively enhance dome- like morphology of human naïve PSCs in HENSM conditions optimized herein.

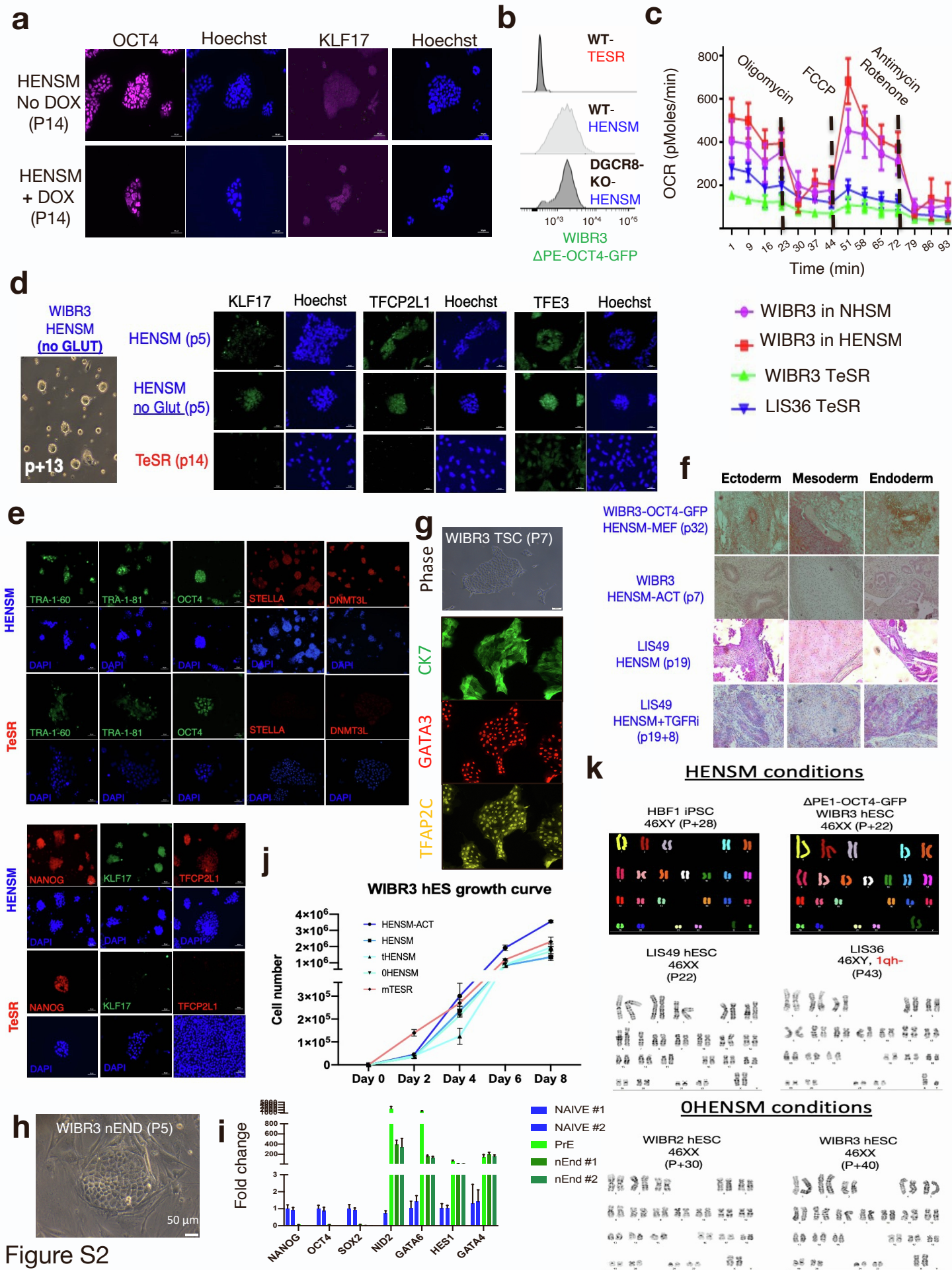
a
OCT4
Hoechst
KLF17
Hoechst
HENSM No DOX (P14)
HENSM + DOX (P14)
b
WT- TESR
WT- HENSM
DGCR8-KO- HENSM
WIBR3 ΔPE-OCT4-GFP
c
OCR (pMoles/min)
Oligomycin
FCCP
Antimycin Rotenone
Time (min)
d
WIBR3 HENSM (no GLUT)
p+13
KLF17
Hoechst
TFCP2L1
TFE3
HENSM (p5)
HENSM no Glut (p5)
TeSR (p14)
WIBR3 in NHSM
WIBR3 in HENSM
WIBR3 TeSR
LIS36 TeSR
e
HENSM
TeSR
TRA-1-60
TRA-1-81
OCT4
STELLA
DNMT3L
DAPI
NANOG
KLF17
TFCP2L1
g
Phase
WIBR3 TSC (P7)
CK7
GATA3
TFAP2C
f
Ectoderm
Mesoderm
Endoderm
WIBR3-OCT4-GFP HENSM-MEF (p32)
WIBR3 HENSM-ACT (p7)
LIS49 HENSM (p19)
LIS49 HENSM+TGFRi (p19+8)
k
HENSM conditions
HBF1 iPSC 46XY (P+28)
ΔPE1-OCT4-GFP WIBR3 hESC 46XX (P+22)
LIS49 hESC 46XX (P22)
LIS36 46XY, 1qh- (P43)
j
WIBR3 hES growth curve
Cell number
HENSM-ACT
HENSM
tHENSM
0HENSM
mTESR
Day 0
Day 2
Day 4
Day 6
Day 8
h
WIBR3 nEND (P5)
50 µm
i
Fold change
NANOG
OCT4
SOX2
NID2
GATA6
HES1
GATA4
NAIVE #1
NAIVE #2
PrE
nEnd #1
nEnd #2
0HENSM conditions
WIBR2 hESC 46XX (P+30)
WIBR3 hESC 46XX (P+40)

Figure S2

Figure S2. Cell characterization in HENSM conditions. Related to Figure 2.

a. Immunostaining for W3G4 before and after DOX validating METTL3 protein downregulation after DOX addition in HENSM. **b.** FACS analysis showing preservation of ΔPE-OCT4-GFP naïve marker expression in both WT and DGCR8 KO human ESCS expanded in HENSM conditions. **c**. Oxygen consumptions rate (OCR) measurement by Seahorse platform in different conditions. **d.** Representative phase contrast and fluorescent images of human cells expanded in HENSM conditions with and without exogenous L-Glutamine (GLUT). TeSR primed human ESCs were used as controls. **e.** Representative immunostaining for pluripotency markers in HENSM conditions are shown for LIS49 hESC line. Primed cells expanded in TeSR conditions are used as controls. **f.** Mature teratoma images are shown following their derivation from the indicated cell lines expanded in the different indicated conditions. Please note that without exception, all teratomas were formed following direct subcutaneous injections after being expanded only in the indicated media condition and without the need for any expansion in other primed conditions *in vitro* before injection. **g**. Phase-contrast image and immunostaining validating TSC identify of a line derived from WIBR3 hESC expanded in HENSM. **h**. Differentiation of WIBR3 naïve hPSCs in HENSM into naïve extra-embryonic endoderm (nEnd) cells. Phase-contrast bright-field image of differentiated nEnd cells on MEFs is shown. **i** RT-qPCR analysis of pluripotency (NANOG,OCT4 and SOX2) and endoderm markers (NID2, GATA6, HES1 and GATA4) in naïve PSC, primitive endoderm (PrE) and naïve endoderm (nEnd) cells illustrating induction of endoderm signatures and loss of pluripotency in differentiated PrE and nEnd cells. Naïve #1 HENSM sample was set as 1. Two independent biological replicates are shown for naive hPSCs and naive endoderm cells. **j**. Representative growth rate curve for different naïve and primed conditions. **k.** Metaphase chromosomal spreads are shown from the indicated human ESC and iPSC lines expanded in HENSM and OHENSM based conditions. Passage numbers are indicated throughout.

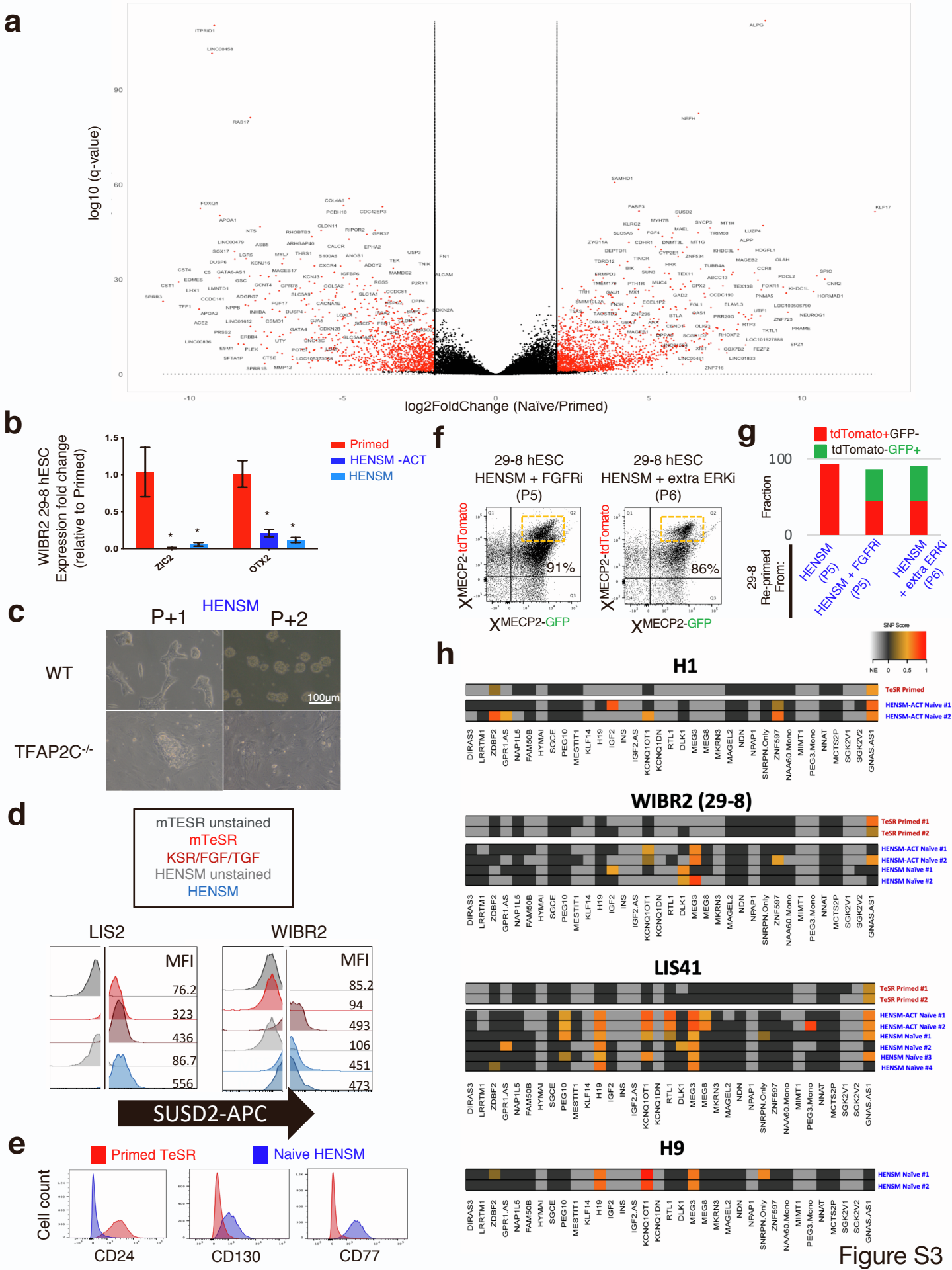
a
log10 (q-value)
log2FoldChange (Naïve/Primed)
b
WIBR2 29-8 hESC
Expression fold change
(relative to Primed)
Primed
HENSM -ACT
HENSM
ZIC2
OTX2
c
HENSM
P+1
P+2
WT
TFAP2C-/-
100µm
d
mTESR unstained
mTeSR
KSR/FGF/TGF
HENSM unstained
HENSM
LIS2
WIBR2
MFI
76.2
323
436
86.7
556
85.2
94
493
106
451
473
SUSD2-APC
e
Primed TeSR
Naive HENSM
Cell count
CD24
CD130
CD77
f
29-8 hESC
HENSM + FGFRi
(P5)
29-8 hESC
HENSM + extra ERKi
(P6)
XMECP2-tdTomato
XMECP2-GFP
91%
86%
g
tdTomato+GFP-
tdTomato-GFP+
Fraction
100
0
29-8
Re-primed
From:
HENSM
(P5)
HENSM + FGFRi
(P5)
HENSM
+ extra ERKi
(P6)
h
SNP Score
H1
TeSR Primed
HENSM-ACT Naïve #1
HENSM-ACT Naïve #2
WIBR2 (29-8)
TeSR Primed #1
TeSR Primed #2
HENSM-ACT Naïve #1
HENSM-ACT Naïve #2
HENSM Naïve #1
HENSM Naïve #2
LIS41
TeSR Primed #1
TeSR Primed #2
HENSM-ACT Naïve #1
HENSM-ACT Naïve #2
HENSM Naïve #1
HENSM Naïve #2
HENSM Naïve #3
HENSM Naïve #4
H9
HENSM Naïve #1
HENSM Naïve #2
DIRAS3
LRRTM1
ZDBF2
GPR1.AS
NAP1L5
FAM50B
HYMAI
SGCE
PEG10
MESTIT1
KLF14
H19
IGF2
INS
IGF2.AS
KCNQ1OT1
KCNQ1DN
RTL1
DLK1
MEG3
MEG8
MKRN3
MAGEL2
NDN
NPAP1
SNRPN.Only
ZNF597
NAA60.Mono
MIMT1
PEG3.Mono
NNAT
MCTS2P
SGK2V1
SGK2V2
GNAS.AS1

Figure S3

Figure S3. Differentially expressed genes between human HENSM naïve and primed states. Related to Figure 3.

a. Volcano plot comparing change in expression of all genes (log2(Naïve HENSM/primed Fold-Change) in x-axis), to their statistic (-log10(q-value) in y-axis). Differentially expressed genes (Fold-change>2(<0.5), p-adjusted<0.1) are marked in red. Extreme genes are highlighted. **b**. RT-PCR validation of expression of ZIC2 and OTX2. *t-test *p* Value < 0.001. **c.** Phase-contrast images showing loss of TFAP2C KO pluripotent cells expansion within 2 passages in HENSM conditions. **d**. FACS staining results on different primed (red colors) and HENSM conditions for SUSD2 expression. MFI values are indicated and compared to matched unstained negative controls. **e.** FACS analysis for expression levels of the indicated surface markers. CD130 and CD77 are induced in HENSM conditions consistent with their previous designation as markers of human naïve pluripotency (Collier et al. Cell Stem Cell 2017). CD24 is depleted in HENSM naïve conditions as expected. **f.** FACS results following using WIBR2 (female 46XX) 29-8 hESC line that carries GFP and tdTomato on each of the X chromosomes in the MECP2 locus. Parental 29-8 clone has the X chromosome carrying GFP allele in the active state, and thus is positive only for GFP and negative for tdTomato in the primed state. Upon transfer to HENSM, HENSM +FGFRi (PD173074 0.75microM) or HENSM-extra ERKi (1.25microM PD0325901), cells turn on both X chromosomes and thus become double positive for both fluorescent markers (GFP and tdTomato). tdTomato-high fraction is highlighted in orange boxed area. **g**. Naïve 29-8 cells were reprimed in FGF/KSR conditions for 3 passages from the different indicated naïve conditions. Random inactivation (presence of both single positive GFP or tdTomato cells) was evident upon additional FGFR signaling inhibition, consistent with a recent report. **h.** SNP based analysis of loss of imprinting (LOI) in hPSCs. Heatmap of biallelic expression including the complete list of imprinted genes in hPSC samples. Genes are arranged according to their genomic proximity. NE - not expressed (FPKM < 0.2).

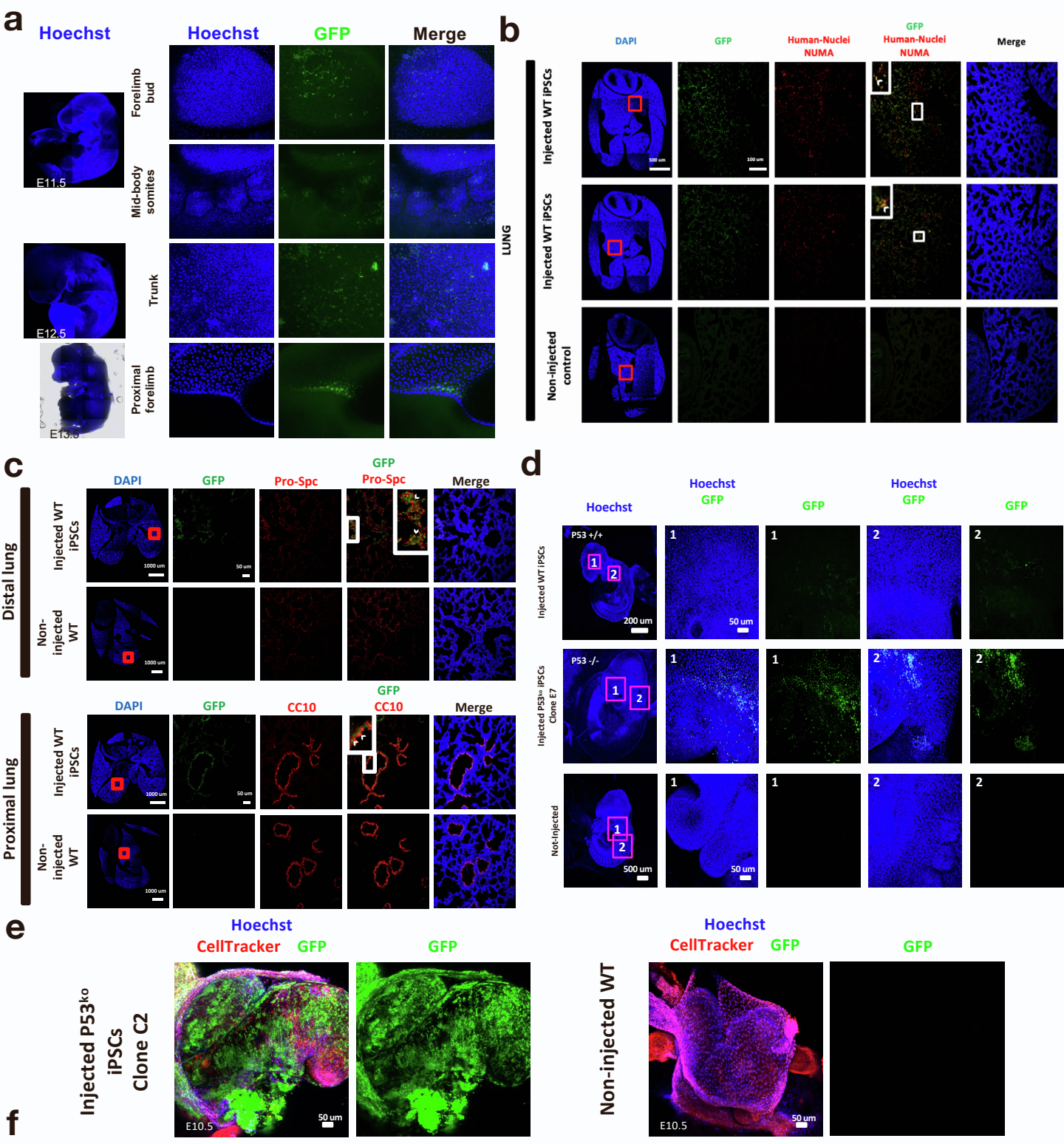

Cell lines	Average chimeric embryos per micro-injection batch	Range % of human cells observed within chimeric mouse embryos	Embryo age for this analysis
Naïve WT hiPSCs	0.8 (n=9)	1-2%	E9.5 – E10.5
Naïve P53 KO hiPSC	3.6 (n=13)	1-20%	E9.5 – E10.5

Figure S4.

Figure S4. P53 depleted human naïve pluripotent stem cells are more competent for interspecies chimerism. Related to Figure 4. **a.** Representative images of whole mount *in toto* microscopy of chimaeric embryos over several developmental stages (E11.5 until E13.5). Panels on the right are zoomed-in regions of tiles on the left side. Hoechst was used as counterstain and anti-GFP staining used to trace human iPSC-derived descendants. **b.** Frozen tissue sections of E17.5 chimaeric embryos were stained for GFP and Human-Nuclei to confirm human origin identity. Non-injected embryos served as negative control. GFP, Human-Nuclei, overlap as well as merged are zoomed-in regions of lung tissue depicted in red squares in the tiles. White arrowheads in insets point out co-localization between GFP and Human-Nuclei. GFP, green fluorescent protein; WT, wild type; iPSC, induced pluripotent stem cell. Tile scale bar 500 um. Zoomed-in scale bar 100 um. **c**. Representative images of frozen tissue sections of E17.5 chimaeric embryos were stained for GFP and Pro-Spc for lung-specific alveolar-surfactant secreting cells. Non-injected embryos served as negative control. GFP, Pro-Spc, overlap as well as merged are zoomed-in regions of lung tissue depicted in red squares in the tiles. White arrowheads in insets point out co-localization between GFP and Pro-Spc or CC10 (Clara-cell 10) lung cell markers. GFP, green fluorescent protein; WT, wild type; Pro-Spc, prosurfactant Protein C. Tile scale bar 1000 um. Zoomed-in scale bar 50 um. **d.** Boost in cell chimerism contribution by depleting P53 in hiPSCs before microinjection. Representative images depicting integration of P53KO GFP-labelled hiPSCs into different locations within developing E9.5/E10.5 mouse embryo in comparison to WT GFP+-cells and non-injected embryos used as negative controls. Red squares in the first column represent zoomed-in areas shown in the following images 1 and 2. Tile scale bar 200 um. Inset scale bar 50 um. **e.** Abnormally developed E10.5 chimaeric embryo due to very high GFP contribution in comparison to non-injected WT embryo lacking any GFP signal. Hoechst and CellTracker were used for counterstaining. Scale bar 50 um. **f.** Summarizing table for outcome of injections of different hiPSCs into mouse embryos.

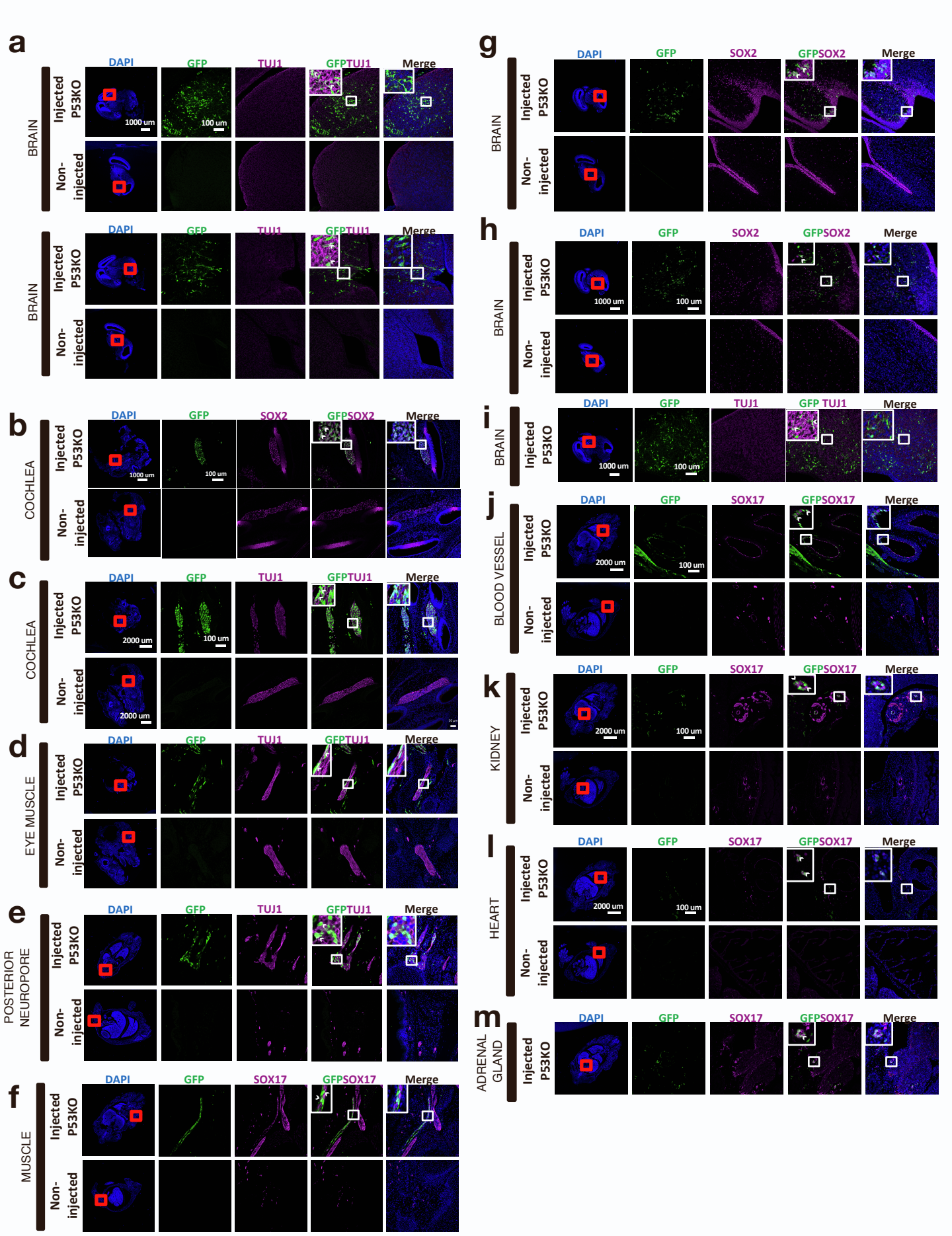
a
BRAIN
Injected P53KO
Non-injected
DAPI
GFP
TUJ1
GFPTUJ1
Merge
1000 um
100 um
BRAIN
Injected P53KO
Non-injected
DAPI
GFP
TUJ1
GFPTUJ1
Merge
b
COCHLEA
Injected P53KO
Non-injected
DAPI
GFP
SOX2
GFPSOX2
Merge
1000 um
100 um
c
COCHLEA
Injected P53KO
Non-injected
DAPI
GFP
TUJ1
GFPTUJ1
Merge
2000 um
100 um
d
EYE MUSCLE
Injected P53KO
Non-injected
DAPI
GFP
TUJ1
GFPTUJ1
Merge
e
POSTERIOR NEUROPORE
Injected P53KO
Non-injected
DAPI
GFP
TUJ1
GFPTUJ1
Merge
f
MUSCLE
Injected P53KO
Non-injected
DAPI
GFP
SOX17
GFPSOX17
Merge
g
BRAIN
Injected P53KO
Non-injected
DAPI
GFP
SOX2
GFPSOX2
Merge
h
BRAIN
Injected P53KO
Non-injected
DAPI
GFP
SOX2
GFPSOX2
Merge
1000 um
100 um
i
BRAIN
Injected P53KO
DAPI
GFP
TUJ1
GFP TUJ1
Merge
1000 um
100 um
j
BLOOD VESSEL
Injected P53KO
Non-injected
DAPI
GFP
SOX17
GFPSOX17
Merge
2000 um
100 um
k
KIDNEY
Injected P53KO
Non-injected
DAPI
GFP
SOX17
GFPSOX17
Merge
2000 um
100 um
l
HEART
Injected P53KO
Non-injected
DAPI
GFP
SOX17
GFPSOX17
Merge
2000 um
100 um
m
ADRENAL GLAND
Injected P53KO
DAPI
GFP
SOX17
GFPSOX17
Merge

Figure S5.

Figure S5. Contribution of GFP labeled P53KO hiPSC-derived progeny to various lineages within chimaeric mouse embryos. Related to Figure 4.

Representative images of IHC staining of injected (upper panels) and non-injected E15.5 mouse embryos (lower panels when included) for (**a**) brain region by TUJ1, (**b,c**) cochlea by SOX2, (**d,e**) eye muscle and posterior neuropore by TUJ1, (**f**) muscle tissue by SOX17, (**g,h**) brain by SOX2, (**i**) brain by TUJ1, (**j,k**) blood vessels and kidney region by SOX17, (**l, m**) heart and adrenal gland regions by SOX17 respectively, are shown. GFP serves as human cell tracer of microinjected P53KO hiPSC, and the developmental markers are used to verify proper integration and acquisition of tissue identity. GFP, TUJ1, SOX2, SOX17 and overlap as well as merged constitute zoomed-in regions of tissues depicted in red squares in the tiles. White arrowheads in insets depict co-localization of GFP and the respective tissue marker. Scale bars for tiles and zoomed-in regions are indicated.

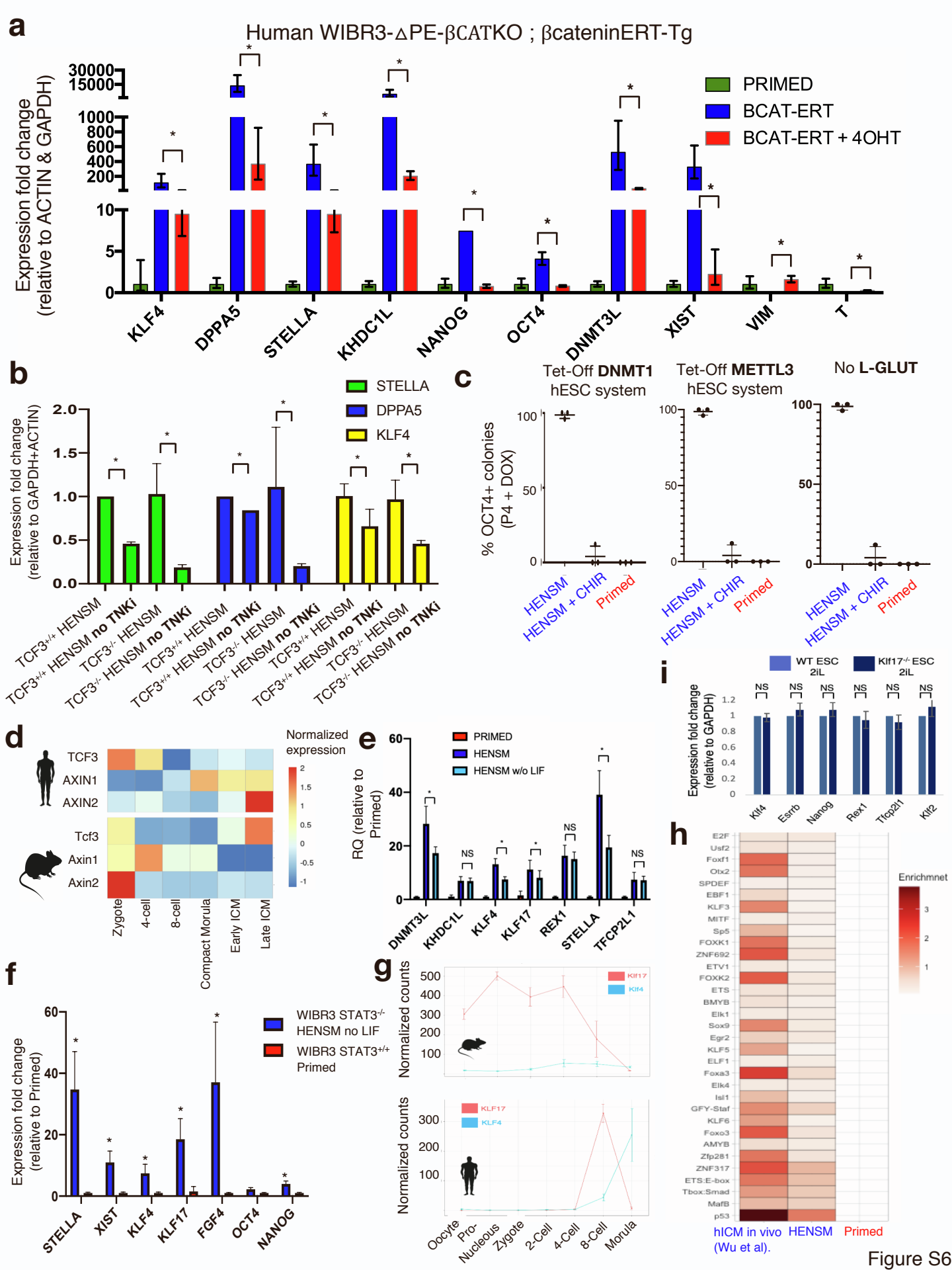
a
Human WIBR3-ΔPE-βCATKO ; βcateninERT-Tg
Expression fold change (relative to ACTIN & GAPDH)
PRIMED
BCAT-ERT
BCAT-ERT + 4OHT
KLF4
DPPA5
STELLA
KHDC1L
NANOG
OCT4
DNMT3L
XIST
VIM
T
b
Expression fold change (relative to GAPDH+ACTIN)
STELLA
DPPA5
KLF4
TCF3+/+ HENSM
TCF3+/+ HENSM no TNKi
TCF3-/- HENSM
TCF3-/- HENSM no TNKi
c
Tet-Off DNMT1 hESC system
Tet-Off METTL3 hESC system
No L-GLUT
% OCT4+ colonies (P4 + DOX)
HENSM
HENSM + CHIR
Primed
d
TCF3
AXIN1
AXIN2
Tcf3
Axin1
Axin2
Normalized expression
Zygote
4-cell
8-cell
Compact Morula
Early ICM
Late ICM
e
PRIMED
HENSM
HENSM w/o LIF
RQ (relative to Primed)
NS
DNMT3L
KHDC1L
KLF4
KLF17
REX1
STELLA
TFCP2L1
i
WT ESC 2iL
Klf17-/- ESC 2iL
Expression fold change (relative to GAPDH)
Klf4
Esrrb
Nanog
Rex1
Tfcp2l1
Klf2
f
Expression fold change (relative to Primed)
WIBR3 STAT3-/- HENSM no LIF
WIBR3 STAT3+/+ Primed
STELLA
XIST
KLF4
KLF17
FGF4
OCT4
NANOG
g
Normalized counts
Klf17
Klf4
KLF17
KLF4
Oocyte
Pro-Nucleous
Zygote
2-Cell
4-Cell
8-Cell
Morula
h
Enrichmnet
hICM in vivo (Wu et al).
HENSM
Primed

Figure S6

Figure S6. Nuclear βCATENIN signaling induces priming of human PSCs. Related to Figure 5.

a. RT-PCR analysis for naïve pluripotency maker expression in Human WIBR3-ΔPE-βCATKO ; βCateninERT-Tg line before and after Tamoxifen addition for 48 hours. Values were normalized to ACTIN and GAPDH. Primed expression levels were set as 1. *t-test *p* Value < 0.01. Naïve pluripotency marker expression was significantly downregulated upon induction of nuclear βCATENIN signaling in human PSCs. **b**. RT-PCR analysis for naïve pluripotency maker expression in the indicated conditions, with and without TNKi, in TCF3 WT and KO hESCs. Values were normalized to ACTIN and GAPDH. *t-test *p* Value < 0.01. $TCF3^{+/+}$ HENSM expression levels were set as 1. **c**. Percentage of OCT4+ cells at P4 from TET-OFF-DNMT1, DNMT1-TET-OFF cell lines and OCT4-GFP cells in the absence of exogenous L-Glut in primed, naïve HENSM, and naïve HENSM supplemented with 1.5μM CHIR99021. **d.** Normalized expression pattern of TCF3 and AXIN1/2 transcripts in mouse and human, as reported in previous single-cell RNA-seq measurement in mouse and human embryos. **e.** RT-PCR analysis for naïve pluripotency maker expression in the indicated naïve and primed conditions, with and without LIF. Values were normalized to ACTIN and GAPDH. Primed expression levels were set as 1. *t-test *p* Value < 0.01; NS- not significant. **f.** RT-PCR analysis for naïve pluripotency maker expression in the indicated lines and conditions. Values were normalized to ACTIN and GAPDH. Primed expression levels were set as 1. *t-test *p* Value < 0.01; NS- not significant. Naïve pluripotency marker remain highly expressed in STAT3 KO ESCs in HENSM conditions, when compared to primed cells that do not express at all these specific markers. **g.** KLF4 and KLF17 relative abundance in pre-implantation stages as measured *in vivo* by scRNA-seq. Please note that KLF17 is not expressed in the mouse ICM (but rather at 2 Cell stage in the mouse), while in humans it is rather upregulated at the morula-ICM stages. **h.** Motif enrichment in human ICM and HENSM commonly enriched accessible chromatin regions. Motif families are indicated at the right. Shades represent enrichment fold-change.

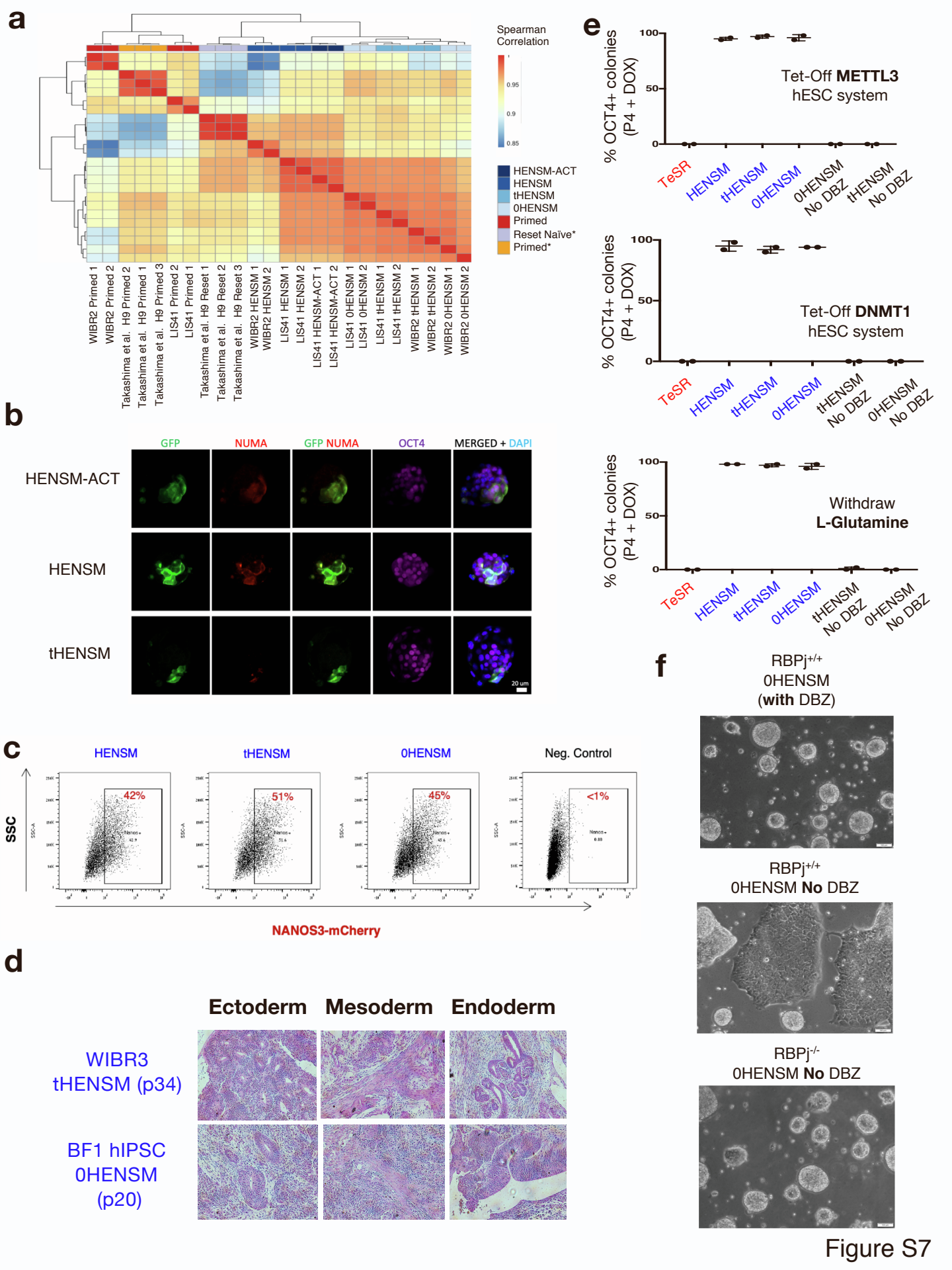
a
Spearman Correlation
1
0.95
0.9
0.85
HENSM-ACT
HENSM
tHENSM
0HENSM
Primed
Reset Naïve*
Primed*
WIBR2 Primed 1
WIBR2 Primed 2
Takashima et al. H9 Primed 2
Takashima et al. H9 Primed 1
Takashima et al. H9 Primed 3
LIS41 Primed 2
LIS41 Primed 1
Takashima et al. H9 Reset 1
Takashima et al. H9 Reset 2
Takashima et al. H9 Reset 3
WIBR2 HENSM 1
WIBR2 HENSM 2
LIS41 HENSM 1
LIS41 HENSM 2
LIS41 HENSM-ACT 1
LIS41 HENSM-ACT 2
LIS41 0HENSM 1
LIS41 0HENSM 2
LIS41 tHENSM 1
LIS41 tHENSM 2
WIBR2 tHENSM 1
WIBR2 tHENSM 2
WIBR2 0HENSM 1
WIBR2 0HENSM 2
e
% OCT4+ colonies (P4 + DOX)
Tet-Off METTL3 hESC system
TeSR
HENSM
tHENSM
0HENSM
0HENSM No DBZ
tHENSM No DBZ
Tet-Off DNMT1 hESC system
Withdraw L-Glutamine
b
GFP
NUMA
GFP NUMA
OCT4
MERGED + DAPI
HENSM-ACT
HENSM
tHENSM
20 um
c
HENSM
tHENSM
0HENSM
Neg. Control
42%
51%
45%
<1%
SSC
NANOS3-mCherry
d
Ectoderm
Mesoderm
Endoderm
WIBR3 tHENSM (p34)
BF1 hIPSC 0HENSM (p20)
f
RBPj+/+ 0HENSM (with DBZ)
RBPj+/+ 0HENSM No DBZ
RBPj-/- 0HENSM No DBZ

Figure S7

Figure S7. Alternative HENSM conditions for human naïve-like PSCs without using ERKi. Related to Figure 7.

a. Spearman correlation matrix of primed samples, along HENSM, HENSM-ACT, tHENSM and 0HENSM samples, as well as previously published naïve and primed samples (Takashima et al, 2014). **b**. Representative immunostaining images of mouse blastocysts 48h after GFP labeled human naïve P53 null hiPSCs expanded in the indicated conditions, were micro-aggregated with mouse 2-Cell embryos. **c**. Competence for human naïve PSCs for differentiating into PGCLCs *in vitro* was assayed for NANOS3-mCherry knock in reporter line expanded for at least 3 passages in HENSM, tHENSM or 0HENSM conditions. Percentages of NANOS3+ cells detected by FACS analysis are shown. **d**. Representative images of teratoma formation from cell expanded in tHENSM and 0HENSM conditions. **e**. Percentage of OCT4-GFP+ cells at P4 from WIBR3-OCT4-GFP cells in HENSM, tHENSM and 0HENSM conditions without METTL3, DNMT1 or exogenously added L-Glutamine. **f.** Phase-contrast images of $RBPj^{+/+}$ and $RBPj^{-/-}$ WIBR3 hESCs upon removal of DBZ from OHENSM conditions.